Chapter 12

Stretch, fold, prune

> **I.1. Introduction to conjugacy problems for diffeomorphisms.** This is a survey article on the area of global analysis defined by differentiable dynamical systems or equivalently the action (differentiable) of a Lie group G on a manifold M. Here Diff(M) is the group of all diffeomorphisms of M and a diffeomorphism is a differentiable map with a differentiable inverse. (. . .) Our problem is to study the global structure, i.e., all of the orbits of M.
>
> —Stephen Smale, *Differentiable Dynamical Systems*

We have learned that the Rössler attractor is very thin, but otherwise the return maps that we found were disquieting – figure 3.3 did not appear to be a one-to-one map. This apparent loss of invertibility is an artifact of projection of higher-dimensional return maps onto their lower-dimensional subspaces. As the choice of a lower-dimensional subspace is arbitrary, the resulting snapshots of return maps look rather arbitrary, too. Such observations beg a question: Does there exist a natural, intrinsic coordinate system in which we should plot a return map?

We shall argue in sect. 12.1 that the answer is yes: The intrinsic coordinates are given by the stable/unstable manifolds, and a return map should be plotted as a map from the unstable manifold back onto the immediate neighborhood of the unstable manifold. In chapter 5 we established that Floquet multipliers of periodic orbits are (local) dynamical invariants. Here we shall show that every equilibrium point and every periodic orbit carries with it stable and unstable manifolds which provide topologically invariant *global* foliation of the state space. They will enable us to partition the state space in a dynamically invariant way, and assign symbolic dynamics itineraries to trajectories.

The topology of stretching and folding fixes the relative spatial ordering of trajectories, and separates the admissible and inadmissible itineraries. We illustrate how this works on Hénon map example 12.3. Determining which symbol sequences are absent, or 'pruned' is a formidable problem when viewed in the state

space, $[x_1, x_2, ..., x_d]$ coordinates. It is equivalent to the problem of determining the location of all homoclinic tangencies, or all turning points of the Hénon attractor. They are dense on the attractor, and show no self-similar structure in the state space coordinates. However, in the 'danish pastry' representation of sect. 12.3 (and the 'pruned danish,' in American vernacular, of sect. 12.4), the pruning problem is visualized as crisply as the New York subway map; any itinerary which strays into the 'pruned region' is banned.

The level is distinctly cyclist, in distinction to the pedestrian tempo of the preceding chapter. Skip most of this chapter unless you really need to get into nitty-gritty details of symbolic dynamics.

fast track:
chapter 13, p. 286

12.1 Goin' global: stable/unstable manifolds

> The complexity of this figure will be striking, and I shall not even try to draw it.
>
> — H. Poincaré, on his discovery of homoclinic tangles, *Les méthodes nouvelles de la méchanique céleste*

The Jacobian matrix J^t transports an infinitesimal neighborhood, its eigenvalues and eigen-directions describing deformation of an initial infinitesimal frame of

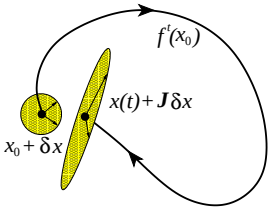

neighboring trajectories into a distorted frame time t later, as in figure 4.1. Nearby trajectories separate exponentially along the unstable directions, approach each other along the stable directions, and creep along the marginal directions.

The fixed point q Jacobian matrix $J(x)$ eigenvectors (5.8) form a rectilinear coordinate frame in which the flow into, out of, or encircling the fixed point is

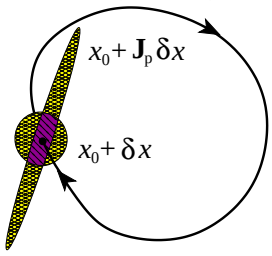

linear in the sense of sect. 4.3.

The continuations of the span of the local stable, unstable eigen-directions into global curvilinear invariant manifolds are called the *stable*, respectively *unstable manifolds*. They consist of all points which march into the fixed point forward,

respectively backward in time

$$\begin{aligned} W^s &= \left\{x \in \mathcal{M} : f^t(x) - x_q \to 0 \text{ as } t \to \infty\right\} \\ W^u &= \left\{x \in \mathcal{M} : f^{-t}(x) - x_q \to 0 \text{ as } t \to \infty\right\} . \end{aligned} \tag{12.1}$$

Eigenvectors $\mathbf{e}^{(i)}$ of the monodromy matrix $J(x)$ play a special role - on them the action of the dynamics is the linear multiplication by Λ_i (for a real eigenvector) along 1-dimensional invariant curve $W^{u,s}_{(i)}$ or spiral in/out action in a 2-D surface (for a complex pair). For $t \to \pm\infty$ a finite segment on $W^s_{(c)}$, respectively $W^u_{(e)}$ converges to the linearized map eigenvector $\mathbf{e}^{(c)}$, respectively $\mathbf{e}^{(e)}$, where $^{(c)}$, $^{(e)}$ stand respectively for 'contracting,' 'expanding.' In this sense each eigenvector defines a (curvilinear) axis of the stable, respectively unstable manifold.

example 12.2
p. 276

Actual construction of these manifolds is the converse of their definition (12.1): one starts with an arbitrarily small segment of a fixed point eigenvector and lets evolution stretch it into a finite segment of the associated manifold. As a periodic point x on cycle p is a fixed point of $f^{T_p}(x)$, the fixed point discussion that follows applies equally well to equilibria and periodic orbits.

Expanding real and positive Floquet multiplier. Consider ith expanding eigenvalue, eigenvector pair $(\Lambda_i, \mathbf{e}^{(i)})$ computed from $J = J_p(x)$ evaluated at a fixed point x,

$$J(x)\mathbf{e}^{(i)}(x) = \Lambda_i \mathbf{e}^{(i)}(x) , \quad x \in \mathcal{M}_p , \quad \Lambda_i > 1 . \tag{12.2}$$

Take an infinitesimal eigenvector $\mathbf{e}^{(i)}(x)$, $\|\mathbf{e}^{(i)}(x)\| = \varepsilon \ll 1$, and its return $\Lambda_i \mathbf{e}^{(i)}(x)$ after one period T_p. Sprinkle the straight interval between $[\varepsilon, \Lambda_i \varepsilon] \subset W^u_{(i)}$ with a large number of points $x^{(k)}$, for example equidistantly spaced on logarithmic scale between $\ln \varepsilon$ and $\ln \Lambda_i + \ln \varepsilon$. The successive returns of these points $f^{T_p}(x^{(k)})$, $f^{2T_p}(x^{(k)})$, $\cdots$, $f^{mT_p}(x^{(k)})$ trace out the $1d$ curve $W^u_{(i)}$ within the unstable manifold. As separations between points tend to grow exponentially, every so often one needs to interpolate new starting points between the rarified ones. Repeat for $-\mathbf{e}^{(i)}(x)$.

Contracting real and positive Floquet multiplier. Reverse the action of the map backwards in time. This turns a contracting direction into an expanding one, tracing out the curvilinear stable manifold $W^s_{(i)}$ as a continuation of $\mathbf{e}^{(i)}$.

Expanding/contracting real negative Floquet multiplier. As above, but every even iterate $f^{2T_p}(x^{(k)})$, $f^{4T_p}(x^{(k)})$, $f^{6T_p}(x^{(k)})$ continues in the direction $\mathbf{e}^{(i)}$, every odd one in the direction $-\mathbf{e}^{(i)}$.

Complex Floquet multiplier pair, expanding/contracting. The complex Floquet multiplier pair $\{\Lambda_j, \Lambda_{j+1} = \Lambda_j^*\}$ has Floquet exponents (4.8) of form $\lambda^{(j)} =$

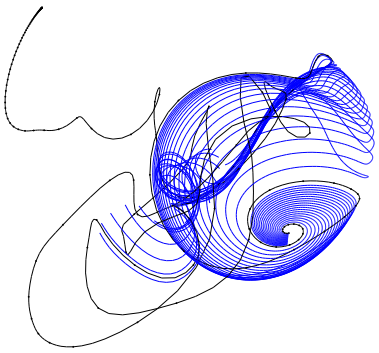

Figure 12.1: A $2d$ unstable manifold obtained by continuation from the linearized neighborhood of a complex eigenvalue pair of an unstable equilibrium of plane Couette flow, a projection from a 61,506-dimensional state space ODE truncation of the (∞-dimensional) Navier-Stokes PDE. (J.F. Gibson, 8 Nov. 2005 blog entry [12.61])

$\mu^{(j)} \pm i\omega^{(j)}$, with the sign of $\mu^{(kj)} \neq 0$ determining whether the linear neighborhood is out / in spiralling. The orthogonal pair of real eigenvectors $\{\mathrm{Re}\,\mathbf{e}^{(j)}, \mathrm{Im}\,\mathbf{e}^{(j)}\}$ spans a plane. $T = 2\pi/\omega^{(j)}$ is the time of one turn of the spiral, $J^T \mathrm{Re}\,\mathbf{e}^{(j)}(x) = |\Lambda_j| \mathrm{Re}\,\mathbf{e}^{(j)}(x)$. As in the real cases above, sprinkle the straight interval between $[\varepsilon, |\Lambda_j|\varepsilon]$ along $\mathrm{Re}\,\mathbf{e}^{(j)}(x)$ with a large number of points $x^{(k)}$. The flow will now trace out the $2d$ invariant manifold as an out / in spiralling strip. Two low-dimensional examples are the unstable manifolds of the Lorenz flow, figure 11.8 (a), and the Rössler flow, figure 11.10 (a). For a highly non-trivial example, see figure 12.1.

The unstable manifolds of a flow are d_u-dimensional. Taken together with the marginally stable direction along the flow, they are rather hard to visualize. A more insightful visualization is offered by $(d-1)$-dimensional Poincaré sections (3.2) with the marginal flow direction eliminated (see also sect. 3.1.2). Stable, unstable manifolds for maps are defined by

$$\begin{aligned} \hat{W}^s &= \left\{ x \in \mathcal{P} : P^n(x) - x_q \to 0 \text{ as } n \to \infty \right\} \\ \hat{W}^u &= \left\{ x \in \mathcal{P} : P^{-n}(x) - x_q \to 0 \text{ as } n \to \infty \right\}, \end{aligned} \tag{12.3}$$

where $P(x)$ is the $(d-1)$-dimensional return map (3.1). In what follows, all invariant manifolds W^u, W^s will be restricted to their Poincaré sections $\hat{W}^u$, $\hat{W}^s$.

example 12.3 p. 277

In general the full state space eigenvectors do not lie in a Poincaré section; the eigenvectors $\hat{\mathbf{e}}^{(j)}$ tangent to the section are given by (5.19). Furthermore, while in the linear neighborhood of fixed point x the trajectories return with approximate periodicity T_p, this is not the case for the globally continued manifolds; $\tau(x)$, or the first return times (3.1) differ, and the $\hat{W}^u_{(j)}$ restricted to the Poincaré section is obtained by continuing trajectories of the points from the full state space curve $W^u_{(j)}$ to the section $\mathcal{P}$.

For long times the unstable manifolds wander throughout the connected ergodic component, and are no more informative than an ergodic trajectory. For example, the line with equitemporal knots in figure 12.1 starts out on a smoothly

curved neighborhood of the equilibrium, but after a 'turbulent' episode decays into an attractive equilibrium point. The trick is to stop continuing an invariant manifold while the going is still good.


fast track:
sect. 12.2, p. 261

Learning where to stop is a bit of a technical exercise, the reader might prefer to skip next section on the first reading.

12.1.1 Parametrization of invariant manifolds


As the flow is nonlinear, there is no 'natural' linear basis to represent it. Wistful hopes like 'POD modes,' 'Karhunen-Loève,' and other linear changes of bases do not cut it. The invariant manifolds are curved, and their coordinatizations are of necessity curvilinear, just as the maps of our globe are, but infinitely foliated and thus much harder to chart.

Let us illustrate this by parameterizing a $1d$ slice of an unstable manifold by its arclength. Sprinkle evenly points $\{x^{(1)}, x^{(2)}, \cdots, x^{(N-1)}\}$ between the equilibrium point $x_q = x^{(0)}$ and point $x = x^{(N)}$, along the $1d$ unstable manifold continuation $x^{(k)} \in \hat{W}^u_{(j)}$ of the unstable $\hat{\mathbf{e}}^{(j)}$ eigendirection (we shall omit the eigendirection label $_{(j)}$ in what follows). Then the arclength from equilibrium point $x_q = x^{(0)}$ to $x = x^{(N)}$ is given by

$$s^2 = \lim_{N\to\infty} \sum_{k=1}^{N} g_{ij}\, dx_i^{(k)} dx_j^{(k)}\,, \qquad dx_i^{(k)} = x_i^{(k)} - x_i^{(k-1)}\,. \tag{12.4}$$

For the lack of a better idea (perhaps the dynamically determined $g = J^\top J$ would be a more natural metric?) let us measure arclength in the Euclidian metric, $g_{ij} = \delta_{ij}$, so

$$s = \lim_{N\to\infty} \left(\sum_{k=1}^{N} \left(dx^{(k)} \right)^2 \right)^{1/2}\,. \tag{12.5}$$

By definition $f^{\tau(x)}(x) \in \hat{W}^u_{(j)}$, so $f^t(x)$ induces a $1d$ map $s(s_0, \tau) = s(f^{\tau(x_0)}(x_0))$.

Turning points are points on the unstable manifold for which the local unstable manifold curvature diverges for forward iterates of the map, i.e., points at which the manifold folds back onto itself arbitrarily sharply. For our purposes, approximate turning points suffice. The $1d$ curve $\hat{W}^u_{(j)}$ starts out linear at x_q, then gently curves until –under the influence of other unstable equilibria and/or periodic orbits– it folds back sharply at 'turning points' and then nearly retraces itself.

This is likely to happen if there is only one unstable direction, as we saw in the Rössler attractor example 11.3, but if there are several, the 'turning point' might get stretched out in the non-leading expanding directions.

The trick is to figure out a good *base segment* to the nearest turning point $L = [0, s_b]$, and after the foldback assign to $s(x,t) > s_b$ the nearest point s on the base segment. If the stable manifold contraction is strong, the 2nd coordinate connecting $s(x,t) \to s$ can be neglected. We saw in example 11.3 how this works. You might, by nature and temperament, take the dark view: Rössler has helpful properties, namely insanely strong contraction along a 1-dimensional stable direction, that are not present in real problems, such as turbulence in a plane Couette flow, and thus the lessons of chapter 11 of no use when it comes to real plumbing. For this reason, both of the training examples to come, the billiards and the Hénon map are of Hamiltonian, phase-space preserving type, and thus as far from being insanely contracting as possible. Yet, to a thoughtful reader, they unfold themselves as pages of a book.

Assign to each d-dimensional point $\hat{x} \in L_q$ a coordinate $s = s(\hat{x})$ whose value is the Euclidean arclength (12.4) to x_q measured along the 1-dimensional $\mathcal{P}_q$ section of the x_q unstable manifold. Next, for a nearby point $\hat{x}_0 \notin L_q$ determine the point $\hat{x}_1 \in L_q$ which minimizes the Euclidean distance $(\hat{x}_0 - \hat{x}_1)^2$, and assign arc length coordinate value $s_0 = s(\hat{x}_1)$ to $\hat{x}_0$. In this way, an approximate 1-dimensional intrinsic coordinate system is built along the unstable manifold. This parametrization is useful if the non–wandering set is sufficiently thin that its perpendicular extent can be neglected, with every point on the non–wandering set assigned the nearest point on the base segment L_q.

Armed with this intrinsic curvilinear coordinate parametrization, we are now in a position to construct a 1-dimensional model of the dynamics on the non–wandering set. If $\hat{x}_n$ is the nth Poincaré section of a trajectory in neighborhood of x_q, and s_n is the corresponding curvilinear coordinate, then $s_{n+1} = f^{\tau_n}(s_n)$ models the full state space dynamics $\hat{x}_n \to \hat{x}_{n+1}$. We approximate $f(s_n)$ by a smooth, continuous 1-dimensional map $f : L_q \to L_q$ by taking $\hat{x}_n \in L_q$, and assigning to $\hat{x}_{n+1}$ the nearest base segment point $s_{n+1} = s(\hat{x}_{n+1})$.

12.2 Horseshoes

If you find yourself mystified by Smale's article abstract quoted on page 261, about 'the action (differentiable) of a Lie group G on a manifold M,' time has come to bring Smale to everyman. If you still remain mystified by the end of this chapter, reading chapter 16 might help; for example, the Liouville operators form a Lie group of symplectic, or canonical transformations acting on the (p, q) manifold.

If a flow is locally unstable but globally bounded, any open ball of initial points will be stretched out and then folded. An example is a 3-dimensional invertible flow sketched in figure 11.10 which returns a Poincaré section of the flow

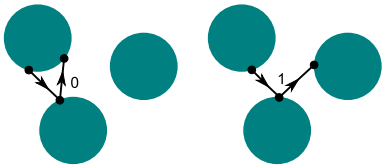

Figure 12.2: Binary labeling of trajectories of the symmetric 3-disk pinball; a bounce in which the trajectory returns to the preceding disk is labeled 0, and a bounce which results in continuation to the third disk is labeled 1.

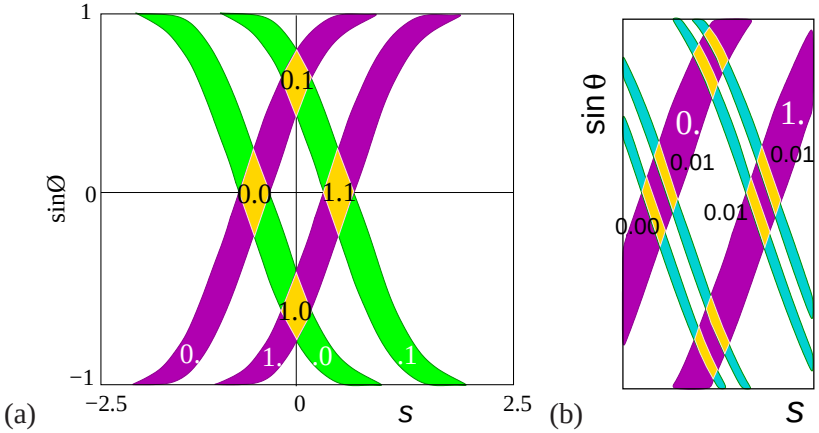

Figure 12.3: The 3-disk game of pinball of figure 11.5, generated by starting from disk 1, preceded by disk 2, coded in binary, as in figure 12.2. (a) Strips $\mathcal{M}_{s_{i..j}}$ which have survived a bounce in the past and will survive a bounce in the future. (b) Iteration corresponds to the decimal point shift; for example, all points in the rectangle [1.01] map into the rectangles [0.10], [0.11] in one iteration.

folded into a 'horseshoe' (we shall belabor this in figure 12.4). We now offer two examples of locally unstable but globally bounded flows which return an initial area stretched and folded into a 'horseshoe,' such that the initial area is intersected at most twice. We shall refer to such mappings with at most 2^n transverse self-intersections at the nth iteration as the *once-folding* maps.

exercise 12.1

The first example is the 3-disk game of pinball figure 11.5, which, for sufficiently separated disks (see figure 11.6), is an example of a complete Smale horseshoe. We start by exploiting its symmetry to simplify it, and then partition its state space by its stable / unstable manifolds.

example 12.4
p. 277

The 3-disk repeller does not really look like a 'horseshoe;' the 'fold' is cut out of the picture by allowing the pinballs that fly between the disks to fall off the table and escape. Next example captures the 'stretch & fold' horseshoe dynamics of return maps such as Rössler's, figure 3.2.

example 12.5
p. 277

What is the significance of the subscript such as $_{.011}$ which labels the $\mathcal{M}_{.011}$ future strip? The two strips $\mathcal{M}_{.0}, \mathcal{M}_{.1}$ partition the state space into two regions labeled by the two-letter alphabet $\mathcal{A} = \{0, 1\}$. $S^+ = .011$ is the *future itinerary* for all $x \in \mathcal{M}_{.011}$. Likewise, for the past strips all $x \in \mathcal{M}_{s_{-m}\cdots s_{-1}s_0.}$ have the *past itinerary* $S^- = s_{-m}\cdots s_{-1}s_0$. Which partition we use to present pictorially the regions that do not escape in m iterations is a matter of taste, as the backward

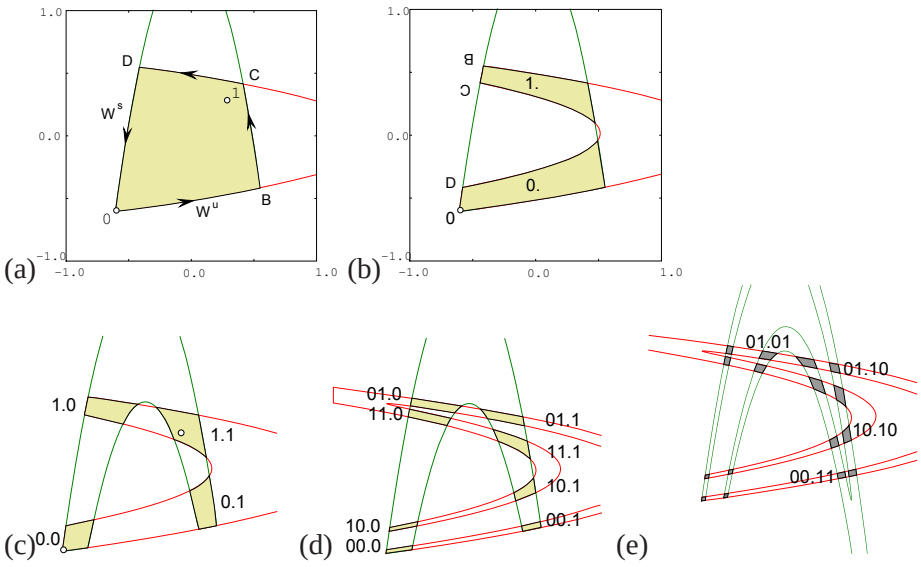

Figure 12.4: The Hénon map (12.20) for $a = 6$, $b = -1$: fixed point $\overline{0}$ with segments of its stable, unstable manifolds W^s, W^u, and fixed point $\overline{1}$. (a) Their intersection bounds the region $\mathcal{M}_{\cdot} = 0BCD$ which contains the non–wandering set Ω. (b) The intersection of the forward image $f(\mathcal{M}_{\cdot})$ with $\mathcal{M}_{\cdot}$ consists of two (future) strips $\mathcal{M}_{0\cdot}$, $\mathcal{M}_{1\cdot}$, with points BCD brought closer to fixed point $\overline{0}$ by the stable manifold contraction. (c) The intersection of the forward image $f(\mathcal{M}_{\cdot})$ with the backward backward $f^{-1}(\mathcal{M}_{\cdot})$ is a four-region cover of Ω. (d) The intersection of the twice-folded forward horseshoe $f^2(\mathcal{M}_{\cdot})$ with backward horseshoe $f^{-1}(\mathcal{M}_{\cdot})$. (e) The intersection of $f^2(\mathcal{M}_{\cdot})$ with $f^{-2}(\mathcal{M}_{\cdot})$ is a 16-region cover of Ω. Iteration yields the complete Smale horseshoe non–wandering set Ω, i.e., the union of all non-wandering points of f, with every forward fold intersecting every backward fold. (P. Cvitanović and Y. Matsuoka)

strips are the preimages of the forward ones

$$\mathcal{M}_{0\cdot} = f(\mathcal{M}_{\cdot 0}), \qquad \mathcal{M}_{1\cdot} = f(\mathcal{M}_{\cdot 1}).$$

Ω, the non–wandering set (2.3) of $\mathcal{M}_{\cdot}$, is the union of all points whose forward and backward trajectories remain trapped for all time, given by the intersections of all images and preimages of $\mathcal{M}$:

$$\Omega = \left\{ x \mid x \in \lim_{m,n\to\infty} f^m(\mathcal{M}_{\cdot}) \bigcap f^{-n}(\mathcal{M}_{\cdot}) \right\}. \tag{12.6}$$

Two important properties of the Smale horseshoe are that it has a *complete binary symbolic dynamics* and that it is *structurally stable*.

For a *complete* Smale horseshoe every forward fold $f^n(\mathcal{M})$ intersects transversally every backward fold $f^{-m}(\mathcal{M})$, so a unique bi-infinite binary sequence can be associated to every element of the non–wandering set. A point $x \in \Omega$ is labeled by the intersection of its past and future itineraries $S(x) = \cdots s_{-2}s_{-1}s_0.s_1s_2\cdots$, where $s_n = s$ if $f^n(x) \in \mathcal{M}_{\cdot s}$, $s \in \{0,1\}$ and $n \in \mathbb{Z}$. remark A.1

The system is said to be *structurally stable* if all intersections of forward and backward iterates of $\mathcal{M}$ remain transverse for sufficiently small perturbations $f \to f + \delta$ of the flow, for example, for slight displacements of the disks in the pinball problem, or sufficiently small variations of the Hénon map parameters a, b. While structural stability is exceedingly desirable, it is also exceedingly rare. About this, more later. section 1.8 section 25.2

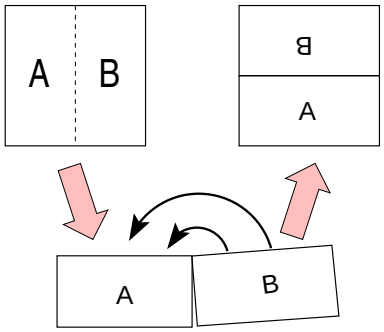

Figure 12.5: Kneading orientation preserving danish pastry: mimic the horsheshoe dynamics of figure 12.6 by: (1) squash the unit square by factor 1/2, (2) stretch it by factor 2, and (3) fold the right half back over the left half.

12.3 Symbol plane

Consider a system for which you have succeeded in constructing a covering symbolic dynamics, such as a well-separated 3-disk system. Now start moving the disks toward each other. At some critical separation a disk will start blocking families of trajectories traversing the other two disks. The order in which trajectories disappear is determined by their relative ordering in space; the ones closest to the intervening disk will be pruned first. Determining inadmissible itineraries requires that we relate the spatial ordering of trajectories to their time ordered itineraries. exercise 12.8

So far we have rules that, given a state space partition, generate a *temporally* ordered itinerary for a given trajectory. Our next task is the converse: given a set of itineraries, what is the *spatial* ordering of corresponding points along the trajectories? In answering this question we will be aided by Smale's visualization of the relation between the topology of a flow and its symbolic dynamics by means of 'horseshoes,' such as figure 12.4.

12.3.1 Kneading danish pastry

The danish pastry transformation, the simplest baker's transformation appropriate to Hénon type mappings, yields a binary coordinatization of all possible periodic points.

The symbolic dynamics of once-folding map is given by the danish pastry transformation. This generates both the longitudinal and transverse alternating binary tree. The longitudinal coordinate is given by the head of a symbolic sequence; the transverse coordinate is given by the tail of the symbolic sequence. The dynamics on this space is given by symbol shift permutations; volume preserving, with 2 expansion and 1/2 contraction.

For a better visualization of 2-dimensional non–wandering sets, fatten the intersection regions until they completely cover a unit square, as in figure 12.7. exercise 12.3
We shall refer to such a 'map' of the topology of a given 'stretch & fold' dynamical system as the *symbol square*. The symbol square is a topologically accurate representation of the non–wandering set and serves as a street map for labeling its exercise 12.4

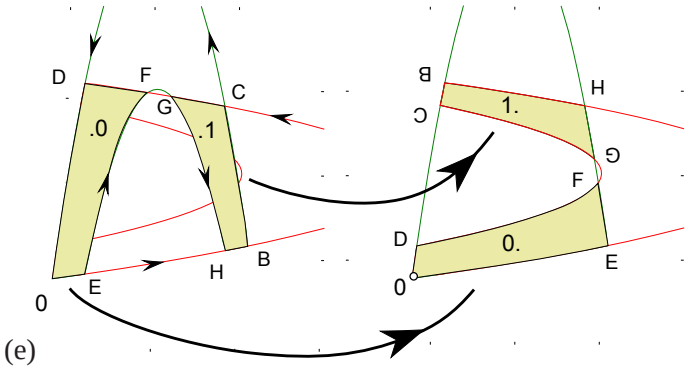

Figure 12.6: The dynamics maps two (past) strips strips $\mathcal{M}_{.0}$, $\mathcal{M}_{.1}$ into two (future) strips $\mathcal{M}_{0.}$, $\mathcal{M}_{1.}$. The corners are labeled to aid visualization. Note that the *BCGH* strip is rotated by 180 degrees. (P. Cvitanović and Y. Matsuoka)

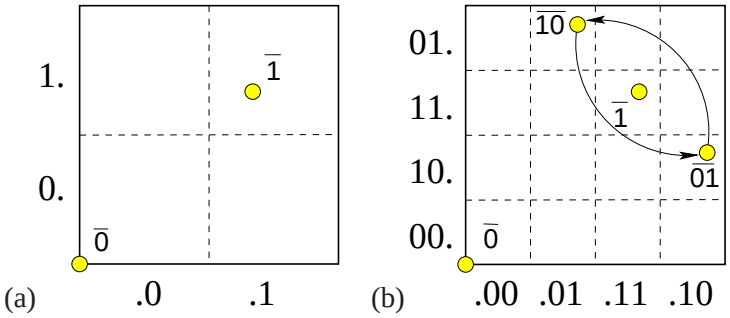

Figure 12.7: Kneading danish pastry: symbol square representation of an orientation preserving once-folding map obtained by fattening the Smale horseshoe intersections of (a) figure 12.6 (b) figure 12.4 into a unit square. Also indicated: the fixed points $\overline{0}$, $\overline{1}$ and the 2-cycle points $\{\overline{01},\overline{10}\}$. In the symbol square the dynamics maps rectangles into rectangles by a decimal point shift.

pieces. Finite memory of m steps and finite foresight of n steps partitions the symbol square into *rectangles* $[s_{-m+1}\cdots s_0.s_1s_2\cdots s_n]$, such as those of figure 12.6. In the binary dynamics symbol square the size of such rectangle is $2^{-m}\times 2^{-n}$; it corresponds to a region of the dynamical state space which contains all points that share common n future and m past symbols. This region maps in a nontrivial way in the state space, but in the symbol square its dynamics is exceedingly simple; all of its points are mapped by the decimal point shift (11.20)

$$\sigma(\cdots s_{-2}s_{-1}s_0.s_1s_2s_3\cdots) = \cdots s_{-2}s_{-1}s_0s_1.s_2s_3\cdots\,, \tag{12.7}$$

Example 12.1 ***A Hénon repeller subshift:*** *(continued from example 12.5) The Hénon map acts on the binary partition as a shift map. Figure 12.6 illustrates action $f(\mathcal{M}_{.0}) = \mathcal{M}_{0.}$. The square* $[01.01]$ *gets mapped into the rectangles* $\sigma[01.01] = [10.1] = \{[10.10],[10.11]\}$*, see figure 12.4 (e). Further examples can be gleaned from figure 12.4.*

As the horseshoe mapping is a simple repetitive operation, we expect a simple relation between the symbolic dynamics labeling of the horseshoe strips, and their relative placement. The symbol square points $\gamma(S^+)$ with future itinerary S^+ are constructed by converting the sequence of s_n's into a binary number by the algorithm (11.9). This follows by inspection from figure 12.9. In order to understand this relation between the topology of horseshoes and their symbolic dynamics, it might be helpful to backtrace to sect. 11.4 and work through and understand first the symbolic dynamics of 1-dimensional unimodal mappings.

Under backward iteration the roles of 0 and 1 symbols are interchanged; $\mathcal{M}_0^{-1}$ has the same orientation as $\mathcal{M}$, while $\mathcal{M}_1^{-1}$ has the opposite orientation. We assign exercise 12.5

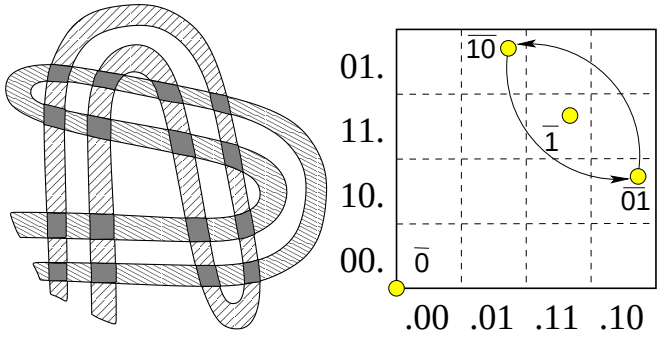

Figure 12.8: Kneading orientation preserving danish pastry: symbol square representation of an orientation preserving once-folding map obtained by fattening the intersections of two forward iterates / two backward iterates of Smale horseshoe into a unit square.

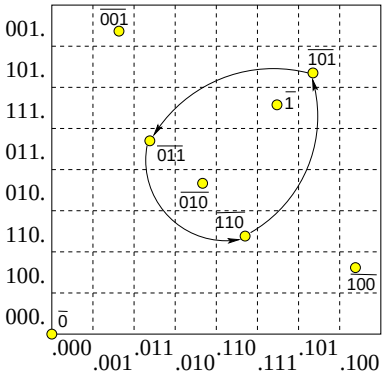

Figure 12.9: Kneading danish pastry: symbol square representation of an orientation preserving once-folding map obtained by fattening the Smale horseshoe intersections of figure 12.4 (e) into a unit square. Also indicated: the fixed points $\overline{0}$, $\overline{1}$, and the 3-cycle points $\{\overline{011},\overline{110},\overline{101}\}$. In the symbol square the dynamics maps rectangles into rectangles by a decimal point shift.

to an *orientation preserving* once-folding map the *past topological coordinate* $\delta = \delta(S^-)$ by the algorithm:

$$
\begin{aligned}
w_{n-1} &= \begin{cases} w_n & \text{if } s_n = 0 \\ 1 - w_n & \text{if } s_n = 1 \end{cases}, \qquad w_0 = s_0 \\
\delta(S^-) &= 0.w_0 w_{-1} w_{-2} \ldots = \sum_{n=1}^{\infty} w_{1-n}/2^n \,. \qquad (12.8)
\end{aligned}
$$

Such formulas are best derived by solitary contemplation of the action of a folding map, in the same way we derived the future topological coordinate (11.9).

The coordinate pair (δ, γ) associates a point (x, y) in the state space Cantor set of figure 12.4 to a point in the symbol square of figure 12.9, preserving the topological ordering. The symbol square $[\delta, \gamma]$ serves as a topologically faithful representation of the non–wandering set of any once-folding map, and aids us in partitioning the set and ordering the partitions for any flow of this type.

fast track:
chapter 13, p. 286

12.4 Prune danish

> Anyone know where I can get a good prune danish in Charlotte? I mean a real NY Jewish bakery kind of prune danish!
>
> — Googled

In general, not all possible symbol sequences are realized as physical trajectories. Trying to get from 'here' to 'there' we might find that a short path is excluded by some obstacle, such as a disk that blocks the path, or a potential ridge. In order to enumerate orbits correctly, we need to *prune* the inadmissible symbol sequences, i.e., describe the grammar of the admissible itineraries.

The complete Smale horseshoe dynamics discussed so far is rather straightforward, and sets the stage for situations that resembles more the real life. A generic once-folding map does not yield a complete horseshoe; some of the horseshoe pieces might be *pruned*, i.e., not realized for particular parameter values of the mapping. In 1 dimension, the criterion for whether a given symbolic sequence is realized by a given unimodal map is easily formulated; any orbit that strays to the right of the value computable from the *kneading sequence* (the orbit of the critical point (11.13)) is pruned. This is a topological statement, independent of a particular unimodal map. Our objective is to generalize this notion to 2-dimensional once-folding maps.

Adjust the parameters of a once-folding map so that the intersection of the backward and forward folds is still transverse, but no longer complete, as in figure 12.10 (a). The utility of the symbol square lies in the fact that the surviving, admissible itineraries still maintain the same relative spatial ordering as for the complete case.

In the example of figure 12.10 the rectangles [10.1], [11.1] have been pruned, and consequently *any* trajectory containing blocks $b_1 = 101$, $b_2 = 111$ is pruned, the symbol dynamics is a subshift of finite type (11.24). We refer to the border of this primary pruned region as the *pruning front*; another example of a pruning front is drawn in figure 12.11 (b). We call it a 'front' as it can be visualized as a border between admissible and inadmissible; any trajectory whose points would fall to the right of the front in figure 12.11 is inadmissible, i.e., pruned. The pruning front is a complete description of the symbolic dynamics of once-folding maps.For now we need this only as a concrete illustration of how pruning rules arise.

In the example at hand there are total of two forbidden blocks 101, 111, so For now we concentrate on this kind of pruning because it is particularly clean and simple.

fast track:
chapter 13, p. 286

Though a useful tool, Markov partitioning is not without drawbacks. One glar-

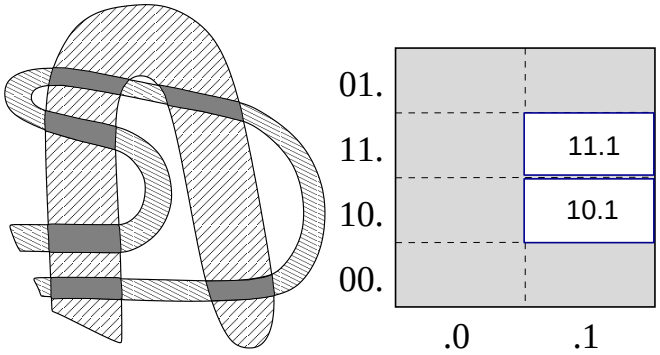

Figure 12.10: (a) An incomplete Smale horseshoe: the inner forward fold does not intersect the outer backward fold. (b) The primary pruned region in the symbol square and the corresponding forbidden binary blocks.

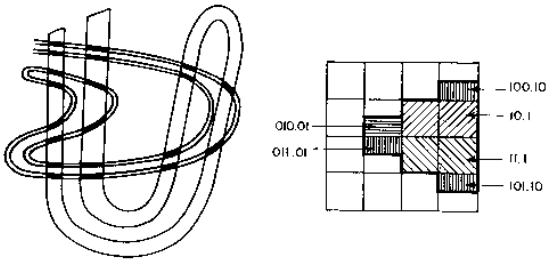

Figure 12.11: (a) An incomplete Smale horseshoe which illustrates (b) the monotonicity of the pruning front: the thick line which delineates the left border of the primary pruned region is monotone on each half of the symbol square. The backward folding in this figure and figure 12.10 is schematic - in invertible mappings there are further missing intersections, all obtained by the forward and backward iterations of the primary pruned region.

ing shortcoming is that Markov partitions are not unique: any of many different partitions might do the job. The $Zn2$- and D_3- equivariant systems that we discuss next offers a simple illustration of different Markov partitioning strategies for the same dynamical system.

12.5 Recoding, symmetries, tilings

In chapter 9.4 we made a claim that if there is a symmetry of dynamics, we must use it. Here we shall show how to use it, on two concrete examples, and in chapter 21 we shall be handsomely rewarded for our labors. First, the simplest example of equivariance, a single 'reflection' $Dn1$ group of example 9A.15.

example 12.7
p. 278

Next, let us take the old pinball game and 'quotient' the state space by the symmetry, or 'desymmetrize.' As the three disks are equidistantly spaced, our game of pinball has a sixfold symmetry. For instance, the cycles $\overline{12}$, $\overline{23}$, and $\overline{13}$ in figure 12.12 are related to each other by rotation by $\pm 2\pi/3$ or, equivalently, by a relabeling of the disks. We exploit this symmetry by recoding, as in (12.19).

exercise 11.1
exercise 12.7

example 12.6
p. 278
exercise 12.8
exercise 14.2

Binary symbolic dynamics has two immediate advantages over the ternary

Table 12.1: Correspondence between the $Zn2$ symmetry reduced cycles $\tilde{p}$ and the full state space periodic orbits p, together with their multiplicities m_p. Also listed are the two shortest cycles (length 6) related by time reversal, but distinct under $Dn1$.

$\tilde{p}$	p	m_p
1	+	2
0	−+	1
01	−− ++	1
001	−++	2
011	−−− +++	1
0001	−+−− +−++	1
0011	−+++	2
0111	−−−− +++++	1
00001	−+−+−	2
00011	−+−−− +−+++	1
00101	−++−− +−−++	1
00111	−+−−− +−+++	1
01011	−−+++	2
01111	−−−−− +++++	1
001011	−++−−− +−−+++	1
001101	−+++−− +−−−++	1

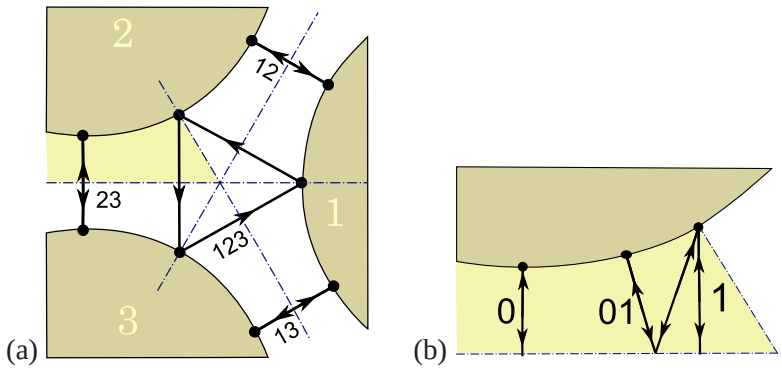

Figure 12.12: The 3-disk game of pinball with the disk radius : center separation ratio a:R = 1:2.5. (a) 2-cycles $\overline{12}$, $\overline{13}$, $\overline{23}$, and 3-cycles $\overline{123}$ and $\overline{132}$ (not drawn). (b) The fundamental domain, i.e., the small 1/6th wedge indicated in (a), consisting of a section of a disk, two segments of symmetry axes acting as straight mirror walls, and an escape gap. The above five cycles restricted to the fundamental domain are the two fixed points $\overline{0}$, $\overline{1}$. See figure 9.3 for cycle $\overline{10}$ and further examples.

one; the prohibition of self-bounces is automatic, and the coding utilizes the symmetry of the 3-disk pinball game in an elegant manner. exercise 11.2

The 3-disk game of pinball is tiled by six copies of the *fundamental domain*, a one-sixth slice of the full 3-disk system, with the symmetry axes acting as reflecting mirrors, see figure 12.12 (b). Every global 3-disk trajectory has a corresponding fundamental domain mirror trajectory obtained by replacing every crossing of a symmetry axis by a reflection. Depending on the symmetry of the full state space trajectory, a repeating binary alphabet block corresponds either to the full periodic orbit or to a relative periodic orbit (examples are shown in figure 12.12 and table 12.2). A relative periodic orbit corresponds to a periodic orbit in the fundamental domain.

Table 12.2 lists some of the shortest binary periodic orbits, together with the corresponding full 3-disk symbol sequences and orbit symmetries. For a number of deep reasons that will be elucidated in chapter 21, life is much simpler in the fundamental domain than in the full system, so whenever possible our computations will be carried out in the fundamental domain.

Table 12.2: D_3 correspondence between the binary labeled fundamental domain prime cycles $\tilde{p}$ and the full 3-disk ternary labeled cycles p, together with the D_3 transformation that maps the end point of the $\tilde{p}$ cycle into the irreducible segment of the p cycle, see example 9.1. White spaces in the above ternary sequences mark repeats of the irreducible segment; for example, the full space 12-cycle 1212 3131 2323 consists of 1212 and its symmetry related segments 3131, 2323. The multiplicity of p cycle is $m_p = 6n_{\tilde{p}}/n_p$. The shortest pair of fundamental domain cycles related by time reversal (but no spatial symmetry) are the 6-cycles $\overline{001011}$ and $\overline{001101}$.

$\tilde{p}$	p	$\mathbf{g}_{\tilde{p}}$	$\tilde{p}$	p	$\mathbf{g}_{\tilde{p}}$
0	1 2	σ_{12}	000001	121212 131313	σ_{23}
1	1 2 3	C	000011	121212 313131 232323	C^2
01	12 13	σ_{23}	000101	121213	e
001	121 232 313	C	000111	121213 212123	σ_{12}
011	121 323	σ_{13}	001011	121232 131323	σ_{23}
0001	1212 1313	σ_{23}	001101	121231 323213	σ_{13}
0011	1212 3131 2323	C^2	001111	121231 232312 313123	C
0111	1213 2123	σ_{12}	010111	121312 313231 232123	C^2
00001	12121 23232 31313	C	011111	121321 323123	σ_{13}
00011	12121 32323	σ_{13}	0000001	1212121 2323232 3131313	C
00101	12123 21213	σ_{12}	0000011	1212121 3232323	σ_{13}
00111	12123	e	0000101	1212123 2121213	σ_{12}
01011	12131 23212 31323	C	0000111	1212123	e
01111	12132 13123	σ_{23}	...	...	...

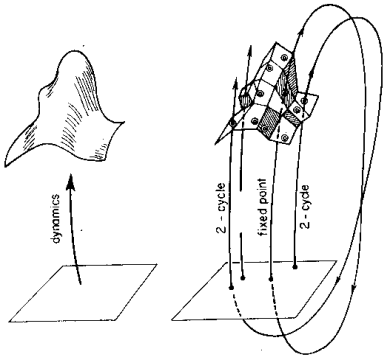

Figure 12.13: Reduction of a continuous-time flow (left frame) to a set of Poincaré maps (right frame), with a point on 1-cycle and the two cycle points of a 2-cycle used as template points.

example 12.8
p. 279

12.6 Charting the state space

In simple examples, such as the Rössler example 3.3, a single Poincaré section suffices, but this is rarely the case for flows of physical interest. In this section (skip it on first reading) we commence a discussion of the general case.

A Poincaré section is constructed by picking a 'template' point $\hat{x}'$ within a state space region of interest, and defining a hypersurface (3.2) that goes through the template point. In theory, this Poincaré section could be any (d–1)-dimensional manifold. In practice, a hyperplane (3.14) is the most convenient, the natural choice for the vector normal to the section being $\hat{n} = v(\hat{x}')$, the velocity field at the

template point $\hat{x}'$. This Poincaré section $\hat{x} \in \mathcal{P}$ is a hyperplane, appendix 6A.5

$$v' \cdot (\hat{x} - \hat{x}') = 0\,, \qquad v' = v(\hat{x}')\,, \tag{12.9}$$

normal to the flow direction v' at the template point $\hat{x}'$. Such section cuts the nearby trajectories transversally, and is a good description of solutions similar to the given template.

So one hyperspace $\mathcal{P}$ will, in general, not suffice. A more insightful picture of the dynamics is obtained by partitioning the state space into N qualitatively distinct regions $\{\mathcal{M}_1, \mathcal{M}_2, \ldots, \mathcal{M}_N\}$ and constructing a Poincaré section per region, global *atlas* of the state space composed of N local Poincaré sections $\mathcal{P}^{(j)}$ section 11.1 or *charts*, each one capturing a neighborhood of a qualitatively prominent state $\hat{x}'^{(j)} \in S$. We shall refer to these states as *templates*, each represented in the state space $\mathcal{M}$ of the system by a *template point* $\{\hat{x}'^{(1)}, \hat{x}'^{(2)}, \cdots, \hat{x}'^{(N)}\}$.

Our Poincaré section is a hyperplane. If we pick another template point $\hat{x}'^{(2)}$, it comes along with its own section hyperplane. The $(d-1)$-dimensional Poincaré sections for an adjacent pair of template intersects in a 'ridge' ('boundary,' 'edge'), a $(d-2)$-dimensional hyperplane, easy to compute. Follow an ant (the sequence of Poincaré map iterates) as it progresses along the Poincaré section $\mathcal{P}^{(1)}$. The moment $(\hat{x}^{(1)}(\tau) - \hat{x}'^{(2)}) \cdot \hat{n}^{(2)}$ changes sign, the ant has crossed the ridge, we switch the Poincaré section, and the ant continues its merry stroll now confined to the $\mathcal{P}^{(2)}$ section. Each Poincaré section $\mathcal{P}^{(j)}$, provides a local chart at $\hat{x}'^{(j)}$ for a neighborhood of an important, qualitatively distinct class of solutions; together they 'Voronoi' tessellate the curved manifold in which the reduced dynamics is replaced by a finite set of mappings between hyperplane tiles. An example is the periodic-orbit implementation of the idea of state space tessellation by neighborhoods of recurrent points, so dear to professional cyclists, illustrated in figure 12.13.

For a given dynamical flow, the physical task is to pick a minimal set of qualitatively distinct templates. The state space might be filled by all kinds of highly unstable, never revisited equilibria and relative periodic orbits. The choice of templates should reflect the dynamically prominent states seen in the long-time simulations of system's dynamics. We have only vague advice on how to pick a single Poincaré section (see sect. 3.1.2), and no advice on how to systematically pick a set of 'good' templates, other than that the associated section tiles should be as large as possible, but still sufficiently small to exclude orbit tangencies, i.e., stop before crossing their section borders (3.6). Ideally, one wold like to pick as few templates as possible in figure 12.13. Once templates are picked, the rest is geometry of hyperplanes, so checking whether the section border is on the far side of the tile edge (ridge between two sections) is a fast, linear computation.

There is a rub, though - you need to know how to pick the neighboring templates. Perhaps a glance at figure 12.13 helps visualize the problem; imagine that the tiles belong to the Poincaré sections through template points on these orbits. One could slide templates along their trajectories until the pairs of straight line

segments connecting neighboring template points are minimized, but that seems a bit arbitrary. At this time we have no advice as how to 'synchronize' the templates relative to each other. The astute reader will instantly recognize this as the problem of 'local gauge invariance' or 'gauge fixing' of Quantum Field Theory and General Relativity.

12.6.1 Navigating the Poincaré-charted state space

Our goal now is to replace the continuous-time dynamics by a set of Poincaré maps between a set of hyperplane sections, as in figure 12.13. The flat hyperplane (3.14) is an *ad hoc* construct; one Poincaré section rarely suffices to capture all of the dynamics of interest. Instead we chart the state space by partitioning it into N qualitatively distinct regions $\{\mathcal{M}_1, \mathcal{M}_2, \ldots, \mathcal{M}_N\}$. Successive trajectory intersections with the set of $(d-1)$-dimensional hypersurfaces $\mathcal{P}_s$ embedded in the d-dimensional state space $\mathcal{M}$, define the set of $(d-1) \to (d-1)$ Poincaré maps section 11.1

$$\begin{aligned} \hat{x}_{n+1} &= P_{s_{n+1}s_n}(\hat{x}_n) = f^{\tau(\hat{x}_n)}(\hat{x}_n) \\ &\hat{x}_{n+1} \in \mathcal{P}^{s_{n+1}}\,,\ \hat{x}_n \in \mathcal{P}^{s_n}\,, \qquad s \in \{1, 2, \ldots, N\}\,. \end{aligned} \tag{12.10}$$

The d-dimensional continuous time flow is thus reduced to discrete time composition

$$P_{s_0 s_1 \cdots s_n} = P_{s_n s_{n-1}} \circ \cdots \circ P_{s_2 s_1} \circ P_{s_1 s_0}$$

of a set of Poincaré maps (12.10) that map the coordinates of Poincaré section $\mathcal{P}_{s_n}$ to those of $\mathcal{P}_{s_{n+1}}$, the next section traversed by a given trajectory.

If a trajectory traverses regions $\mathcal{M}_{s_0} \to \mathcal{M}_{s_1} \to \cdots \to \mathcal{M}_{s_n}$, the sequence $s_0 s_1 \cdots s_n = s_n \leftarrow \cdots \leftarrow s_1 \leftarrow s_0$ is said to be *admissible*. The *return map* section 11.6 P_{s_0} from section $\mathcal{P}_{s_0}$ to itself has a contribution from any admissible returning (periodic, $s_n = s_0$) sequence of compositions

$$P_{s_0 s_1 \cdots s_{n-1} s_0} = P_{s_0 s_{n-1}} \circ \cdots \circ P_{s_2 s_1} \circ P_{s_1 s_0} \tag{12.11}$$

The next example offers an unambiguous set of such Poincaré sections which chapter 11 do double duty, providing us both with an exact representation of dynamics in terms of maps, and with a symbolic dynamics, a subject that we will return to in chapter 11.

example 12.9 p. 279

Billiard dynamics is exceptionally simple - free flight segments, followed by specular reflections at boundaries, with billiard boundaries the obvious choice as Poincaré sections. For a general flow one is never so lucky. Also, so far we have discussed only flows with a 1 continuous parameter (the time). The general case of N-parameter continuous symmetries we postpone to chapter 10.

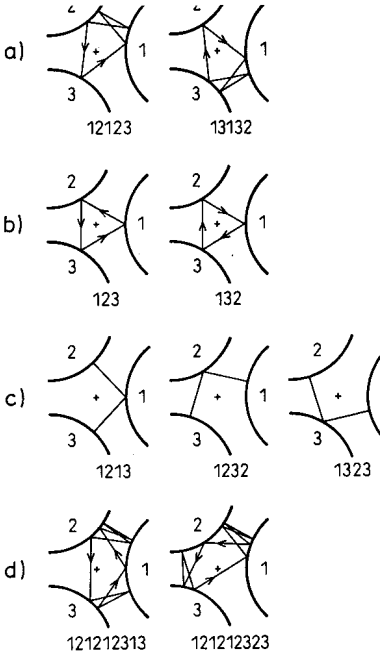

Figure 12.14: Some examples of 3-disk cycles: (a) $\overline{12123}$ and $\overline{13132}$ are mapped into each other by the flip across 1 axis. Similarly (b) $\overline{123}$ and $\overline{132}$ are related by flips, and (c) $\overline{1213}$, $\overline{1232}$ and $\overline{1323}$ by rotations. (d) The cycles $\overline{121212313}$ and $\overline{121212323}$ are related by rotation *and* time reversal. These symmetries are discussed in chapter 9.4. (From ref. [3.1])

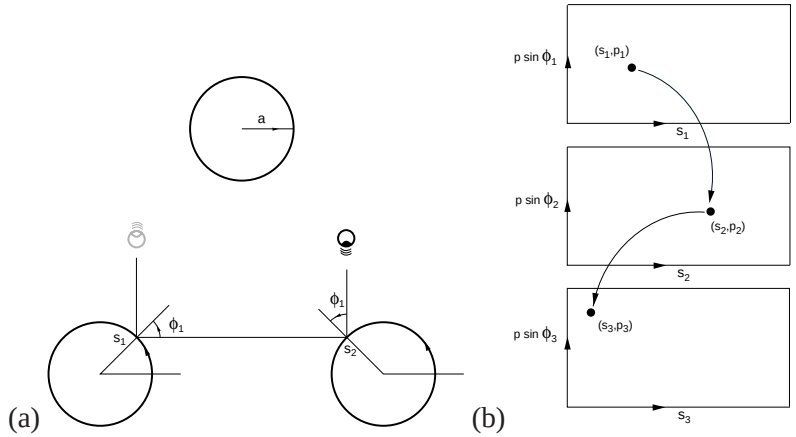

Figure 12.15: (a) Poincaré section coordinates for the 3-disk game of pinball. (b) Collision sequence $(s_1, p_1) \mapsto (s_2, p_2) \mapsto (s_3, p_3)$ from the boundary of a disk to the boundary of the next disk is coded by the Poincaré maps sequence $P_{3\leftarrow 2}P_{2\leftarrow 1}$.

Résumé

In the preceding and this chapter we start with a *d*-dimensional state space and end with a 1-dimensional return map description of the dynamics. The arc-length parametrization of the unstable manifold maintains the 1-to-1 relation of the *full d*-dimensional state space dynamics and its 1-dimensional return-map representation. To high accuracy *no information about the flow is lost* by its 1-dimensional return map description. We explain why Lorenz equilibria are heteroclinically connected (it is not due to the symmetry), and how to generate all periodic orbits of Lorenz flow up to given length. This we do, in contrast to the rest of the thesis, without any group-theoretical jargon to blind you with.

For 1-dimensional maps the folding point is the critical point, and easy to determine. In higher dimensions, the situation is not so clear - one can attempt to determine the (fractal set of) folding points by looking at their higher iterates - due to the contraction along stable manifolds, the fold gets to be exponentially

sharper at each iterate. In practice this set is essentially uncontrollable for the same reason the flow itself is chaotic - exponential growth of errors. We prefer to determine a folding point by bracketing it by longer and longer cycles which can be determined accurately using variational methods of chapter 29, irrespective of their period.

For a generic dynamical system a subshift of finite type is the exception rather than the rule. Its symbolic dynamics can be arbitrarily complex; even for the logistic map the grammar is finite only for special parameter values. Only some repelling sets (like our game of pinball) and a few purely mathematical constructs (called Anosov flows) are structurally stable - for most systems of interest an infinitesimal perturbation of the flow destroys and/or creates an infinity of trajectories, and specification of the grammar requires determination of pruning blocks of arbitrary length. The repercussions are dramatic and counterintuitive; for example, the transport coefficients such as the deterministic diffusion constant of sect. 25.2 are emphatically *not* smooth functions of the system parameters. The importance of symbolic dynamics is often under appreciated; as we shall see in chapters 20 and 23, the existence of a finite grammar is the crucial prerequisite for construction of zeta functions with nice analyticity properties. This generic lack of structural stability is what makes nonlinear dynamics so hard.

section 25.2

The conceptually simpler finite subshift Smale horseshoes suffice to motivate most of the key concepts that we shall need for time being. Our strategy is akin to bounding a real number by a sequence of rational approximants; we converge toward the non–wandering set under investigation by a sequence of self-similar Cantor sets. The rule that everything to one side of the pruning front is forbidden is striking in its simplicity: instead of pruning a Cantor set embedded within some larger Cantor set, the pruning front cleanly cuts out a *compact* region in the symbol square, and that is all - there are no additional pruning rules. A 'self-similar' Cantor set (in the sense in which we use the word here) is a Cantor set equipped with a *subshift of finite type* symbol dynamics, i.e., the corresponding grammar can be stated as a finite number of pruning rules, each forbidding a finite subsequence $\_s_1 s_2 \ldots s_n\_$. Here the notation $\_s_1 s_2 \ldots s_n\_$ stands for n consecutive symbols $s_1 1$, s_2, ..., s_n, preceded and followed by arbitrary symbol strings.

The symbol square is a useful tool in transforming topological pruning into pruning rules for inadmissible sequences; those are implemented by constructing transition matrices and/or graphs, see chapters 14 and 15.

Commentary

Remark 12.1 Stable/unstable manifolds. For pretty hand-drawn pictures of invariant manifolds, see Abraham and Shaw [9A.1]. Construction of invariant manifolds by map iteration is described in Simo [12.34]. Fixed point stable / unstable manifolds and their homoclinic and heteroclinic intersections can be computed using DsTool [12.58, 12.59, 12.60]. Unstable manifold turning points were utilized in refs. [12.12, 22.2, 22.3, 12.31, 12.32, 12.33] to partition state space and prune inadmissible symbol sequences. The arclength parameterized return maps were introduced by Christiansen *et al.* [12.62], and

utilized in ref. [**?**] Even though no dynamical system has been studied more exhaustively than the Lorenz equations, the analysis of sect. 11.2 is new. The desymmetrization follows Gilmore and Lettelier [9A.4], but the key new idea is taken from Christiansen *et al.* [12.62]: the arc-length parametrization of the unstable manifold maintains the 1-to-1 relation of the *full d*-dimensional state space dynamics and its 1-dimensional return-map representation, in contrast to 1-dimensional *projections* of the (d–1)-dimensional Poincaré section return maps previously deployed in the literature. In other words, to high accuracy *no information about the flow is lost* by its 1-dimensional return map description.

Remark 12.2 Smale horseshoe. S. Smale understood clearly that the crucial ingredient in the description of a chaotic flow is the topology of its non–wandering set, and he provided us with the simplest visualization of such sets as intersections of Smale horseshoes. In retrospect, much of the material covered here can already be found in Smale's fundamental paper [1.27], but an engineer or a scientist who has run into a chaotic time series in his laboratory might not know that he is investigating the action (differentiable) of a Lie group G on a manifold M, and that the Lefschetz trace formula is the way to go.

We have tried to explain the geometric picture the best we could in the static text format, but there is no substitute for dynamics but the dynamics itself. We found Demidov's "Chaotic maps" [12.65] simulations of the Hénon map particularly helpful in explaining how horsheshoes partition the non–wandering sets.

Remark 12.3 Pruning fronts. The 'partition conjecture' is due to Grassberger and Kantz [29.3]. The notion of a pruning front and the 'pruning-front conjecture' was formulated by Cvitanović *et al.* [12.12], and developed by K.T. Hansen for a number of dynamical systems in his Ph.D. thesis [12.22] and a series of papers [12.23]-[12.27]. The 'multimodal map approximation' is described in the K.T. Hansen thesis [12.22]. Hansen's thesis is still the most accessible exposition of the pruning theory and its applications. Detailed studies of pruning fronts are carried out in refs. [12.13, **?**, 12.14]; ref. [29.5] is the most detailed study carried out so far. The rigorous theory of pruning fronts has been developed by Y. Ishii [12.18, 12.19] for the Lozi map, and A. de Carvalho [12.16, 12.17] in a very general setting. Beyond the orbit pruning and its infinity of admissible unstable orbits, an attractor of Hénon type may also own an infinity of attractive orbits coexisting with the strange attractor [12.20, 12.21]. We offer heuristic arguments and numerical evidence that the coexistence of attractive orbits does not destroy the strange attractor/repeller, which is also in this case described by the 2-dimensional danish pastry plot.

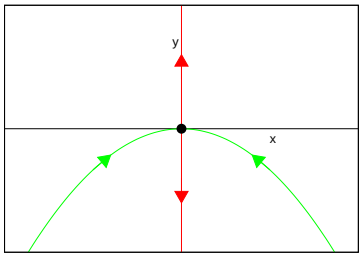

Figure 12.16: The stable/unstable manifolds of the equilibrium $(x_q, x_q) = (0, 0)$ of 2-dimensional flow (12.12).

12.7 Examples

Example 12.2 ***A simple stable/unstable manifolds pair:*** *Consider the 2-dimensional ODE system*

$$\frac{dx}{dt} = -x, \quad \frac{dy}{dt} = y + x^2 \,, \tag{12.12}$$

The flow through a point $x(0) = x_0, y(0) = y_0$ *can be integrated*

$$x(t) = x_0\, e^{-t}, \quad y(t) = (y_0 + x_0^2/3)\, e^{t} - x_0^2\, e^{-2t}/3 \,. \tag{12.13}$$

Linear stability of the flow is described by the stability matrix

$$\mathbf{A} = \begin{pmatrix} -1 & 0 \\ 2x & 1 \end{pmatrix} . \tag{12.14}$$

The flow is hyperbolic, with a real expanding/contracting eigenvalue pair $\lambda_1 = 1$, $\lambda_2 = -1$, *and area preserving. The right eigenvectors at the point* (x, y)

$$\mathbf{e}^{(1)} = \begin{pmatrix} 0 \\ 1 \end{pmatrix}, \qquad \mathbf{e}^{(2)} = \begin{pmatrix} 1 \\ -x \end{pmatrix} . \tag{12.15}$$

can be obtained by acting with the projection operators (see example C.3 Decomposition of 2-dimensional vector spaces*)*

$$\mathbf{P}_i = \frac{\mathbf{A} - \lambda_j \mathbf{1}}{\lambda_i - \lambda_j} : \qquad \mathbf{P}_1 = \begin{pmatrix} 0 & 0 \\ x & 1 \end{pmatrix}, \quad \mathbf{P}_2 = \begin{pmatrix} 1 & 0 \\ -x & 0 \end{pmatrix} \tag{12.16}$$

on an arbitrary vector. Matrices $\mathbf{P}_i$ *are orthonormal and complete.*

The flow has a degenerate pair of equilibria at $(x_q, y_q) = (0, 0)$, *with eigenvalues (stability exponents),* $\lambda_1 = 1$, $\lambda_2 = -1$, *eigenvectors* $\mathbf{e}^{(1)} = (0, 1)$, $\mathbf{e}^{(2)} = (1, 0)$. *The unstable manifold is the* y *axis, and the stable manifold is given by (see figure 12.16)*

$$y_0 + \frac{1}{3}x_0^2 = 0 \Rightarrow y(t) + \frac{1}{3}x(t)^2 = 0 \,. \tag{12.17}$$

(N. Lebovitz)

exercise to return: p. **??**

Example 12.3 ***A section at a fixed point with a complex Floquet multiplier pair:*** *(continued from example 3.1) The simplest choice of a Poincaré section for a fixed (or periodic) point x_q with a complex Floquet multiplier pair is the plane $\mathcal{P}$ specified by the fixed point (located at the tip of the vector x_q) and the eigenvector $\mathrm{Im}\,\mathbf{e}^{(k)}$ perpendicular to the plane. A point x is in the section $\mathcal{P}$ if it satisfies the condition*

$$(x - x_q) \cdot \mathrm{Im}\,\mathbf{e}^{(k)} = 0\,. \tag{12.18}$$

In the neighborhood of x_q the spiral out/in motion is in the $\{\mathrm{Re}\,\mathbf{e}^{(k)}, \mathrm{Im}\,\mathbf{e}^{(k)}\}$ plane, and thus guaranteed to be cut by the Poincaré section $\mathcal{P}$ normal to $\mathbf{e}^{(k)}$. click to return: p. **??**

Example 12.4 ***Recoding 3-disk dynamics in binary.*** *(continued from example 11.2) The $\mathcal{A} = \{1, 2, 3\}$ symbolic dynamics for 3-disk system is neither unique, nor necessarily the smartest one - before proceeding it pays to quotient the symmetries of the dynamics in order to obtain a more efficient description. We do this in a quick way here, and redo it in more detail in sect. 12.5.*

As the three disks are equidistantly spaced, the disk labels are arbitrary; what is important is how a trajectory evolves as it hits subsequent disks, not what label the starting disk had. We exploit this symmetry by recoding*, in this case replacing the absolute disk labels by relative symbols, indicating the type of the collision. For the 3-disk game of pinball there are two topologically distinct kinds of collisions, figure 12.2:*

exercise 11.1
exercise 12.7

$$s_i = \begin{cases} 0 & : \quad \textit{pinball returns to the disk it came from} \\ 1 & : \quad \textit{pinball continues to the third disk}\,. \end{cases} \tag{12.19}$$

In the binary *recoding of the 3-disk symbolic dynamics the prohibition of self-bounces is automatic. If the disks are sufficiently far apart there are no further restrictions on symbols, the symbolic dynamics is complete, and* all *binary sequences (see table 15.1) are admissible.* exercise 11.2

It is intuitively clear that as we go backward in time (reverse the velocity vector), we also need increasingly precise specification of $x_0 = (s_0, p_0)$ in order to follow a given past itinerary. Another way to look at the survivors after two bounces is to plot $\mathcal{M}_{s_1 . s_2}$, the intersection of $\mathcal{M}_{. s_2}$ with the strips $\mathcal{M}_{s_1 .}$ obtained by time reversal (the velocity changes sign $\sin\phi \to -\sin\phi$). $\mathcal{M}_{s_1 . s_2}$, figure 12.3 (a), is a 'rectangle' of nearby trajectories which have arrived from disk s_1 and are heading for disk s_2. (continued in example 12.6) click to return: p. **??**

Example 12.5 ***A Hénon repeller complete horseshoe:*** *(continued from example 3.6) Consider 2-dimensional* Hénon map exercise 3.5

$$(x_{n+1}, y_{n+1}) = (1 - ax_n^2 + by_n, x_n)\,. \tag{12.20}$$

If you start with a small ball of initial points centered around the fixed point x_0, and iterate the map, the ball will be stretched and squashed along the unstable manifold W_0^u. Iterated backward in time,

$$(x_{n-1}, y_{n-1}) = (y_n, -b^{-1}(1 - ay_n^2 - x_n))\,, \tag{12.21}$$

this small ball of initial points traces out the stable manifold W_0^s. Their intersections enclose the region $\mathcal{M}_{.}$, figure 12.4 (a). Any point outside W_0^s border of $\mathcal{M}_{.}$ escapes

to infinity forward in time, while –by time reversal– any point outside W_0^u border arrives from infinity back in paste. In this way the unstable - stable manifolds define topologically, invariant and optimal initial region $\mathcal{M}_{..}$; all orbits that stay confined for all times are confined to $\mathcal{M}_{..}$.

The Hénon map models qualitatively the Poincaré section return map of figure 11.10. For $b = 0$ the Hénon map reduces to the parabola (11.3), and, as shown in sects. 3.3 and 29.1, for $b \neq 0$ it is kind of a fattened parabola; by construction, it takes a rectangular initial area and returns it bent as a horseshoe. Parameter a controls the amount of stretching, while the parameter b controls the amount of compression of the folded horseshoe. For definitiveness, fix the parameter values to $a = 6$, $b = -1$; the map is then strongly stretching but area preserving, the furthest away from the strongly dissipative examples discussed in sect. 11.2. The map is quadratic, so it has 2 fixed points $x_0 = f(x_0)$, $x_1 = f(x_1)$ indicated in figure 12.4 (a). For the parameter values at hand, they are both unstable.

Iterated one step forward, the region $\mathcal{M}_{..}$ is stretched and folded into a Smale *horseshoe drawn in figure 12.4 (b). Label the two forward intersections $f(\mathcal{M}_{..}) \cap \mathcal{M}_{..}$ by $\mathcal{M}_{s.}$, with $s \in \{0, 1\}$. The horseshoe consists of the two strips $\mathcal{M}_{0.}, \mathcal{M}_{1.}$, and the bent segment that lies entirely outside the W_0^s line. As all points in this segment escape to infinity under forward iteration, this region can safely be cut out and thrown away.*

Iterated one step backwards, the region $\mathcal{M}_{..}$ is again stretched and folded into a horseshoe, figure 12.4 (c). As stability and instability are interchanged under time reversal, this horseshoe is transverse to the forward one. Again the points in the horseshoe bend wander off to infinity as $n \to -\infty$, and we are left with the two (past) strips $\mathcal{M}_{.0}, \mathcal{M}_{.1}$. Iterating two steps forward we obtain the four strips $\mathcal{M}_{11.}, \mathcal{M}_{01.}, \mathcal{M}_{00.}, \mathcal{M}_{10.}$, and iterating backwards we obtain the four strips $\mathcal{M}_{.00}, \mathcal{M}_{.01}, \mathcal{M}_{.11}, \mathcal{M}_{.10}$ transverse to the forward ones just as for 3-disk pinball game figure 12.2. Iterating three steps forward we get an 8 strips, and so on ad infinitum. *(continued in example 12.1)* click to return: p. **??**

Example 12.6 ***Recoding ternary symbolic dynamics in binary:*** *Given a ternary sequence and labels of 2 preceding disks, rule (12.19) fixes the subsequent binary symbols. Here we list an arbitrary ternary itinerary, and the corresponding binary sequence:*

$$\begin{array}{rcl} \textit{ternary} & : & 3\ 1\ 2\ 1\ 3\ 1\ 2\ 3\ 2\ 1\ 2\ 3\ 1\ 3\ 2\ 3 \\ \textit{binary} & : & \cdot\ 1\ 0\ 1\ 0\ 1\ 1\ 0\ 1\ 0\ 1\ 1\ 0\ 1\ 0 \end{array} \tag{12.22}$$

The first 2 disks initialize the trajectory and its direction; $3 \mapsto 1 \mapsto 2 \mapsto \cdots$. Due to the 3-disk symmetry the six distinct 3-disk sequences initialized by 12, 13, 21, 23, 31, 32 respectively have the same weights, the same size state space partitions, and are coded by a single binary sequence. (continued in example 12.8) click to return: p. **??**

Example 12.7 C_2 ***recoded:*** *Assume that each orbit is uniquely labeled by an infinite string $\{s_i\}$, $s_i \in \{+, -\}$ and that the dynamics is C_2-equivariant under the $+ \leftrightarrow -$ interchange. Periodic orbits separate into two classes, the self-dual configurations $+-$, $++--$, $+++---$, $+--+-++-$, $\cdots$, with multiplicity $m_p = 1$, and the pairs $+$, $-$, $++-$, $--+$, $\cdots$, with multiplicity $m_p = 2$. For example, as there is no absolute distinction between the 'left' or the 'right' lobe of the Lorenz attractor, figure 3.4 (a), the Floquet multipliers satisfy $\Lambda_+ = \Lambda_-$, $\Lambda_{++-} = \Lambda_{+--}$, and so on.* exercise 9A.1 exercise 21.6

The symmetry reduced labeling $\rho_i \in \{0,1\}$ is related to the full state space labeling $s_i \in \{+,-\}$ by

$$\begin{aligned} &\text{If} \quad s_i = s_{i-1} \quad \text{then} \quad \rho_i = 1 \\ &\text{If} \quad s_i \neq s_{i-1} \quad \text{then} \quad \rho_i = 0 \end{aligned} \tag{12.23}$$

For example, the fixed point $\overline{+} = \cdots + + + + \cdots$ maps into $\cdots 111 \cdots = \overline{1}$, and so does the fixed point $\overline{-}$. The 2-cycle $\overline{-+} = \cdots - + - + \cdots$ maps into fixed point $\cdots 000 \cdots = \overline{0}$, and the 4-cycle $\overline{-++-} = \cdots - - + + - - + + \cdots$ maps into 2-cycle $\cdots 0101 \cdots = \overline{01}$. A list of such reductions is given in table 12.1. click to return: p. **??**

Example 12.8 D_3 ***recoded - 3-disk game of pinball:*** *(continued from example 12.6) The D_3 recoding can be worked out by a glance at figure 12.12 (a) (continuation of example 9A.16). For the symmetric 3-disk game of pinball the fundamental domain is bounded by a disk segment and the two adjacent sections of the symmetry axes that act as mirrors (see figure 12.12 (b)). The three symmetry axes divide the space into six copies of the fundamental domain. Any trajectory on the full space can be pieced together from bounces in the fundamental domain, with symmetry axes replaced by flat mirror reflections. The binary $\{0,1\}$ reduction of the ternary three disk $\{1,2,3\}$ labels has a simple geometric interpretation, figure 12.2: a collision of type 0 reflects the projectile to the disk it comes from (back–scatter), whereas after a collision of type 1 projectile continues to the third disk. For example, $\overline{23} = \cdots 232323 \cdots$ maps into $\cdots 000 \cdots = \overline{0}$ (and so do $\overline{12}$ and $\overline{13}$), $\overline{123} = \cdots 12312 \cdots$ maps into $\cdots 111 \cdots = \overline{1}$ (and so does $\overline{132}$), and so forth. Such reductions for short cycles are given in table 12.2, figure 12.12 and figure 9A.7.* click to return: p. **??**

Example 12.9 ***Pinball game, Poincaré dissected.*** *(continued from sect. 1.4 and chapter 8) A phase-space orbit is fully specified by its position and momentum at a given instant, so no two distinct phase-space trajectories can intersect. The configuration space trajectories, however, can and do intersect, in rather unilluminating ways, as e.g. in figure 12.14 (d), and it can be rather hard to perceive the systematics of orbits from their configuration space shapes. The problem is that we are looking at the projections of 4-dimensional state space trajectories onto a 2-dimensional configuration subspace. A much clearer picture of the dynamics is obtained by constructing a set of Poincaré sections.*

Suppose that the pinball has just bounced off disk 1. Depending on its position and outgoing angle, it could proceed to either disk 2 or 3. Not much happens in between the bounces–the ball just travels at constant velocity along a straight line–so we can reduce the 4-dimensional flow to a 2-dimensional map $P_{\sigma_k \leftarrow \sigma_j}$ that maps the coordinates (Poincaré section $\mathcal{P}_1$) of the pinball from one disk edge to another. Just after the moment of impact the trajectory is defined by s_n, the arc-length position of the nth bounce along the billiard wall, and $p_n = p \sin\phi_n$ the outgoing momentum component parallel to the billiard wall at the point of impact, figure 12.15 (a). These coordinates exercise 8.7 *(due to Birkhoff) are smart, as they conserve the phase-space volume. Trajectories originating from one disk can hit either of the other two disks, or escape without further ado. We label the survivor state space regions $\mathcal{P}_{12}, \mathcal{P}_{13}$. In terms of the three Poincaré sections, one for each disk, the dynamics is reduced to the set of six maps*

$$(s_{n+1}, p_{n+1}) = P_{\sigma_{n+1} \leftarrow \sigma_n}(s_n, p_n), \qquad \sigma \in \{1,2,3\} \tag{12.24}$$

from the boundary of a disk to the boundary of the next disk, figure 12.15 (b). The explicit form of this map is easily written down, see example 8.1, but much more economical is the symmetry quotiented version of chapter 9.4 which replaces the above 6 forward maps by a return map *pair P_0, P_1.* click to return: p. **??**

Exercises

12.1. **A Smale horseshoe.** The Hénon map of example 3.6

$$\begin{bmatrix} x' \\ y' \end{bmatrix} = \begin{bmatrix} 1 - ax^2 + by \\ x \end{bmatrix} \tag{12.25}$$

maps the $[x, y]$ plane into itself - it was constructed by Hénon [3.6] in order to mimic the Poincaré section of once-folding map induced by a flow like the one sketched in figure 11.10. For definitiveness fix the parameters to $a = 6$, $b = -1$.

a) Draw a rectangle in the (x, y) plane such that its nth iterate by the Hénon map intersects the rectangle 2^n times.

b) Construct the inverse of the (12.25).

c) Iterate the rectangle back in the time; how many intersections are there between the n forward and m backward iterates of the rectangle?

d) Use the above information about the intersections to guess the (x, y) coordinates for the two fixed points, a 2-periodic point, and points on the two distinct 3-cycles from table 15.1. The exact periodic points are computed in exercise 13.10.

12.2. **A simple stable/unstable manifolds pair.** Integrate flow (12.12), verify (12.13). Check that the projection matrices $\mathbf{P}_i$ (12.16) are orthonormal and complete. Use them to construct right and left eigenvectors; check that they are mutually orthogonal. Explain why is (12.17) the equation for the stable manifold. (N. Lebovitz)

12.3. **Kneading Danish pastry.** Write down the $(x, y) \to (x, y)$ mapping that implements the baker's map

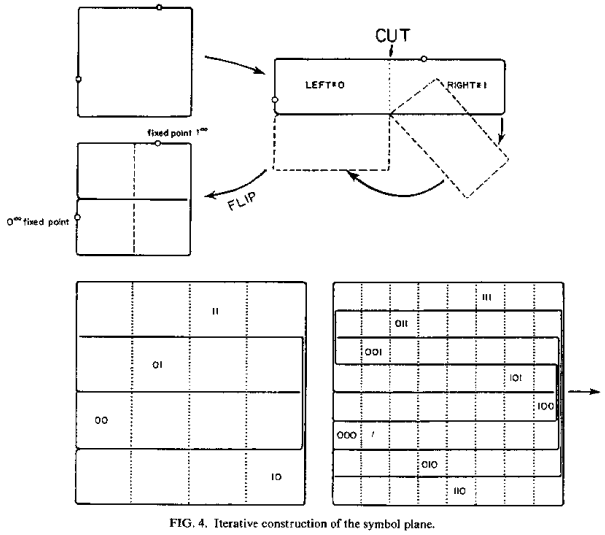

FIG. 4. Iterative construction of the symbol plane.

Figure: *Kneading danish pastry: symbol square representation of an orientation reversing once-folding map obtained by fattening the Smale horseshoe intersections of figure 12.4 into a unit square. In the symbol square the dynamics maps rectangles into rectangles by a decimal point shift.* together with the inverse mapping.

Sketch a few rectangles in symbol square and their forward and backward images. (Hint: the mapping is very much like the tent map (11.4)).

12.4. **Kneading danish without flipping.** The baker's map of exercise 12.3 includes a flip - a map of this type is called an orientation reversing once-folding map. Write down the $(x, y) \to (x, y)$ mapping that implements an orientation preserving baker's map (no flip; Jacobian determinant = 1). Sketch and label the first few folds of the symbol square.

12.5. **Orientation reversing once-folding map.** By adding a reflection around the vertical axis to the horseshoe map g we get the orientation reversing map $\tilde{g}$ shown in the second Figure above. $\tilde{Q}_0$ and $\tilde{Q}_1$ are oriented as Q_0 and Q_1, so the definition of the future topological coordinate γ is identical to the γ for the orientation preserving horseshoe. The inverse intersections $\tilde{Q}_0^{-1}$ and $\tilde{Q}_1^{-1}$ are oriented so that $\tilde{Q}_0^{-1}$ is opposite to Q, while $\tilde{Q}_1^{-1}$ has the same orientation as Q. Check that the past topological coordinate δ is given by

$$w_{n-1} = \begin{cases} 1 - w_n & \text{if } s_n = 0 \\ w_n & \text{if } s_n = 1 \end{cases}, \qquad w_0 = s_0$$

$$\delta(x) \quad = \quad 0.w_0 w_{-1} w_{-2} \ldots = \sum_{n=1}^{\infty} w_{1-n}/2^n \quad (12.26)$$

12.6. **Infinite symbolic dynamics.** Let σ be a function that returns zero or one for every infinite binary string: $\sigma : \{0,1\}^{\mathbb{N}} \to \{0,1\}$. Its value is represented by $\sigma(\epsilon_1, \epsilon_2, \ldots)$ where the ϵ_i are either 0 or 1. We will now define an operator $\mathcal{T}$ that acts on observables on the space of binary strings. A function a is an observable if it has bounded variation, that is, if

$$||a|| = \sup_{\{\epsilon_i\}} |a(\epsilon_1, \epsilon_2, \ldots)| < \infty \,.$$

For these functions

$$\begin{aligned} \mathcal{T}a(\epsilon_1, \epsilon_2, \ldots) \quad &= \quad a(0, \epsilon_1, \epsilon_2, \ldots)\sigma(0, \epsilon_1, \epsilon_2, \ldots) \\ &\quad + a(1, \epsilon_1, \epsilon_2, \ldots)\sigma(1, \epsilon_1, \epsilon_2, \ldots) \,. \end{aligned}$$

(a) (easy) Consider a finite version T_n of the operator $\mathcal{T}$:

$$\begin{aligned} &T_n a(\epsilon_1, \epsilon_2, \ldots, \epsilon_{1,n}) = \\ &\quad a(0, \epsilon_1, \epsilon_2, \ldots, \epsilon_{n-1})\sigma(0, \epsilon_1, \epsilon_2, \ldots, \epsilon_{n-1}) + \\ &\quad a(1, \epsilon_1, \epsilon_2, \ldots, \epsilon_{n-1})\sigma(1, \epsilon_1, \epsilon_2, \ldots, \epsilon_{n-1}) \,. \end{aligned}$$

Show that T_n is a $2^n \times 2^n$ matrix. Show that its trace is bounded by a number independent of n.

(b) (medium) With the operator norm induced by the function norm, show that $\mathcal{T}$ is a bounded operator.

(c) (hard) Show that $\mathcal{T}$ is not trace class.

12.7. **3-disk fundamental domain cycles.** (continued from exercise 9A.1) Try to sketch $\overline{0}$, $\overline{1}$, $\overline{01}$, $\overline{001}$, $\overline{011}$, $\cdots$. in the fundamental domain, and interpret the symbols $\{0,1\}$ by relating them to topologically distinct types of collisions. Compare with table 12.2. Then try to sketch the location of periodic points in the Poincaré section of the billiard flow. The point of this exercise is that while in the configuration space longer cycles look like a hopeless jumble, in the Poincaré section they are clearly and logically ordered. The Poincaré section is always to be preferred to projections of a flow onto the configuration space coordinates, or any other subset of state space coordinates which does not respect the topological organization of the flow.

12.8. **3-disk pruning.** (Not easy) Show that for 3-disk game of pinball the pruning of orbits starts at $R : a = 2.04821419\ldots$, figure 11.6. (K.T. Hansen)

References

[12.1] E. Hopf, *Ergodentheorie* (Chelsea Publ. Co., New York 1948).

[12.2] T. Bedford, M.S. Keane and C. Series, eds., *Ergodic Theory, Symbolic Dynamics and Hyperbolic Spaces* (Oxford Univ. Press, Oxford, 1991).

[12.3] M.S. Keane, *Ergodic theory and subshifts of finite type*, in ref. [12.2].

[12.4] B. Kitchens, "Symbolic dynamics, group automorphisms and Markov partition," in *Real and Complex Dynamical Systems,* B. Branner and P. Hjorth, ed. (Kluwer, Dordrecht, 1995).

[12.5] R. Bowen, "Markov partitions for Axiom A diffeomorphisms," *Amer. J. Math.* **92**, 725 (1970).

[12.6] R. Bowen, *Periodic orbits for hyperbolic flows*, Amer. J. Math. **94**, 1-30 (1972).

[12.7] R. Bowen, *Symbolic dynamics for hyperbolic flows*, Amer. J. Math. **95**, 429-460 (1973).

[12.8] R. Bowen and O.E. Lanford, "Zeta functions of restrictions," pp. 43-49 in *Proceeding of the Global Analysis* (A.M.S., Providence 1968).

[12.9] V.M. Alekseev and M.V. Jakobson, "Symbolic dynamics and hyperbolic dynamical systems," *Phys. Reports* **75**, 287 (1981).

[12.10] A. Manning, "Axiom A diffeomorphisms have rational zeta function," *Bull. London Math. Soc.* **3**, 215 (1971).

[12.11] W. Thurston, "On the geometry and dynamics of diffeomorphisms of surfaces," *Bull. Amer. Math. Soc.* **19**, 417 (1988).

[12.12] P. Cvitanović, G.H. Gunaratne and I. Procaccia, *Phys. Rev.* **A 38**, 1503 (1988).

[12.13] G. D'Alessandro, P. Grassberger, S. Isola and A. Politi, "On the topology of the Hénon Map," *J. Phys.* **A 23**, 5285 (1990).

[12.14] F. Giovannini and A. Politi, "Generating partitions in Hénon-type maps," *Phys. Lett.* **A 161**, 333 (1992);

[12.15] G. D'Alessandro, S. Isola and A. Politi,
"Geometric properties of the pruning front," *Prog. Theor. Phys.* **86**, 1149 (1991).

[12.16] A. de Carvalho, "Pruning fronts and the formation of horseshoes," *Ergod. Theor. Dynam. Syst.* **19**, 851 (1999).

[12.17] A. de Carvalho and T. Hall, "How to prune a horseshoe," *Nonlinearity* **15**, R19 (2002).

[12.18] Y. Ishii, "Towards a kneading theory for Lozi mappings. I. A solution of the pruning front conjecture and the first tangency problem," *Nonlinearity* **10**, 731 (1997).

[12.19] Y. Ishii, "Towards a kneading theory for Lozi Mappings. II: Monotonicity of the topological entropy and Hausdorff dimension of attractors," Comm. Math. Phys, 190, 375-394 (1997).

[12.20] S.E. Newhouse, *Topology* **13**, 9 (1974).

[12.21] S.E. Newhouse, *Publ. Math. IHES* **50**, 101 (1979).

[12.22] K.T. Hansen, *Symbolic Dynamics in Chaotic Systems*, Ph.D. thesis (Univ. of Oslo, 1994);
`ChaosBook.org/projects/KTHansen/thesis`.

[12.23] K.T. Hansen, *CHAOS* **2**, 71 (1992).

[12.24] K.T. Hansen, *Nonlinearity* **5**.

[12.25] K.T. Hansen, *Nonlinearity* **5**.

[12.26] P. Cvitanović and K.T. Hansen, "Symbolic dynamics and Markov partitions for the stadium billiard," *J. Stat. Phys.*, (accepted 1996, revised version still not resubmitted); `arXiv:chao-dyn/9502005`.

[12.27] K.T. Hansen, *Symbolic dynamics IV; a unique partition of maps of Hénon type*, in preparation.

[12.28] Fa-Geng Xie and Bai-Lin Hao, "Counting the number of periods in one-dimensional maps with multiple critical points," *Physica A* **202**, 237 (1994).

[12.29] V. Franceschini and L. Russo, *J. Stat. Phys.* **25**, 757 (1981).

[12.30] G. D'Alessandro and A. Politi, "Hierarchical approach to complexity ...," *Phys. Rev. Lett.* **64**, 1609 (1990).

[12.31] F. Christiansen and A. Politi, "A generating partition for the standard map," *Phys. Rev. E.* **51**, 3811 (1995); arXiv:chao-dyn/9411005.

[12.32] F. Christiansen and A. Politi, "Symbolic encoding in symplectic maps," *Nonlinearity* **9**, 1623 (1996).

[12.33] F. Christiansen and A. Politi, "Guidelines for the construction of a generating partition in the standard map," *Physica D* **109**, 32 (1997).

[12.34] C. Simo, "On the analytical and numerical approximation of invariant manifolds," in D. Baenest and C. Froeschlé, Les Méthodes Modernes de la Mécanique Céleste (Goutelas 1989), p. 285.

[12.35] C. Simo, in *Dynamics and Mission Design Near Libration Points*, Vol. 1-4, (World Sci. Pub., Monograph Ser. Math., 2000-2001).

[12.36] Y. Lan and P. Cvitanović, "Unstable recurrent patterns in Kuramoto-Sivashinsky dynamics," *Phys. Rev. E* **78**, 026208 (2004); arXiv:0804.2474.

[12.37] T. Hall, "Fat one-dimensional representatives of pseudo-Anosov isotopy classes with minimal periodic orbit structure," *Nonlinearity* **7**, 367 (1994).

[12.38] P. Cvitanović and K.T. Hansen, "Symbolic dynamics of the wedge billiard," Niels Bohr Inst. preprint, unpublished (Nov. 1992)

[12.39] P. Cvitanović and K.T. Hansen, "Bifurcation structures in maps of Hénon type," *Nonlinearity* **11**, 1233 (1998).

[12.40] R.W. Easton, "Trellises formed by stable and unstable manifolds in plane," *Trans. Amer. Math. Soc.***294**, 2 (1986).

[12.41] V. Rom-Kedar, "Transport rates of a class of two-dimensional maps and flows," *Physica D* **43**, 229 (1990).

[12.42] V. Daniels, M. Vallières and J-M. Yuan, "Chaotic scattering on a double well: Periodic orbits, symbolic dynamics, and scaling," *Chaos* **3**, 475 (1993).

[12.43] P.H. Richter, H.-J. Scholz and A. Wittek, "A Breathing Chaos," *Nonlinearity* **1**, 45 (1990).

[12.44] F. Hofbauer, "Periodic points for piecewise monotone transformations," *Ergod. The. and Dynam. Sys.* **5**, 237 (1985).

[12.45] F. Hofbauer, "Piecewise invertible dynamical systems," *Prob. Th. Rel. Fields* **72**, 359 (1986).

[12.46] K.T. Hansen, "Pruning of orbits in 4-disk and hyperbola billiards," *CHAOS* **2**, 71 (1992).

[12.47] G. Troll, "A devil's staircase into chaotic scattering," *Pysica D* **50**, 276 (1991)

[12.48] P. Grassberger, "Toward a quantitative theory of self-generated complexity," *Int. J. Theor. Phys* **25**, 907 (1986).

[12.49] D.L. Rod, *J. Diff. Equ.* **14**, 129 (1973).

[12.50] R.C. Churchill, G. Pecelli and D.L. Rod, *J. Diff. Equ.* **17**, 329 (1975).

[12.51] R.C. Churchill, G. Pecelli and D.L. Rod, in G. Casati and J. Ford, eds., *Como Conf. Proc. on Stochastic Behavior in Classical and Quantum Hamiltonian Systems* (Springer, Berlin 1976).

[12.52] R. Mainieri, Ph.D. thesis, New York Univ. (1990); *Phys. Rev.* **A 45**, 3580 (1992)

[12.53] M.J. Giannoni and D. Ullmo, "Coding chaotic billiards: I. Non-compact billiards on a negative curvature manifold," *Physica* **D 41**, 371 (1990).

[12.54] D. Ullmo and M.J. Giannoni, "Coding chaotic billiards: II. Compact billiards defined on the pseudosphere," *Physica* **D 84**, 329 (1995).

[12.55] H. Solari, M. Natiello and G.B. Mindlin, "Nonlinear Physics and its Mathematical Tools," (IOP Publishing Ltd., Bristol, 1996).

[12.56] R. Gilmore, "Topological analysis of chaotic time series data," *Revs. Mod. Phys.* **70**, 1455 (1998).

[12.57] E. Hille, *Analytic function theory II*, (Ginn and Co., Boston 1962).

[12.58] A. Back, J. Guckenheimer, M. R. Myers, F. J. Wicklin and P. A. Worfolk, "DsTool: Computer assisted exploration of dynamical systems," *Notices of the AMS* **39**, 303 (1992).

[12.59] B. Krauskopf and H. M. Osinga, "Investigating torus bifurcations in the forced Van der Pol oscillator," pp. 199–208 in E. Doedel and L. Tuckerman, eds., *Numerical Methods for Bifurcation Problems and Large-Scale Dynamical Systems*, *The IMA Volumes in Mathematics and its Applications* **119** (Springer-Verlag, New York 2000).

[12.60] J. P. England, B. Krauskopf and H. M. Osinga, "Computing one-dimensional stable and unstable sets of planar maps without the inverse," *J. Applied Dynam. Systems* **3**, 161 (2004).

[12.61] J. F. Gibson, J. Halcrow, and P. Cvitanović, "Visualizing the geometry of state-space in plane Couette flow," *J. Fluid Mech.* **611**, 107 (2008); `arXiv:0705.3957`.

[12.62] F. Christiansen, P. Cvitanović and V. Putkaradze, "Hopf's last hope: spatiotemporal chaos in terms of unstable recurrent patterns," *Nonlinearity* **10**, 55 (1997); `arXiv:chao-dyn/9606016`.

[12.63] S.E. Newhouse, *Topology* **13**, 9 (1974).

[12.64] S.E. Newhouse, *Publ. Math. IHES* **50**, 101 (1979).

[12.65] E. Demidov, "Chaotic maps," www.ibiblio.org/e-notes